

Wideband model of man-made HF noise and interference

John J. Lemmon

Institute for Telecommunication Sciences, U.S. Department of Commerce, Boulder, Colorado

Abstract. A mathematical model of the waveform generated by man-made high frequency (HF) noise and interference is presented and discussed. The model is based on wideband (800 kHz) recordings of the noise and interference at various frequencies in the HF band. Representative examples of first- and higher-order statistics of the measured waveforms are described, including probability distributions of the envelope and phase of the noise and interference in the time and frequency domains, power spectra, autocorrelation functions, and level crossing distributions. The statistics of waveforms generated by the model closely resemble the statistics of the measured data.

1. Introduction

Over the past several years the application of spread spectrum technology and digital signal processing techniques to high frequency (HF) communication systems has generated considerable interest in HF communications over wide bandwidths (of the order of 1 MHz or more). Since many questions exist concerning the performance of these new wideband systems, it is important to have HF channel models for theoretical predictions of system performance and for laboratory performance measurements using channel simulators.

The HF channel models and channel simulators currently in widespread use are based on narrowband measurements. For example, the model described by the *International Radio Consultative Committee (CCIR)* [1986] is based on limited measurements over bandwidths of 12 kHz or less. It could be misleading to use such models to assess system performance over bandwidths of hundreds of kilohertz or more, and it is therefore necessary to develop channel models that are valid over much wider bandwidths.

The propagation of HF signals in the ionosphere comprises a rich variety of phenomena that can have a deleterious effect on system performance. The development of a model that describes these propagation effects on wideband HF signals has been developed and discussed elsewhere [Vogler and Hoffmeyer, 1993]. However, the importance of these effects notwithstanding, what often determine the limits of radio system performance are the additive

disturbances in the channel, i.e., the noise and interference, which can be quite severe in the HF band (3–30 MHz). A wideband model of the noise and interference has therefore been developed for use in channel simulators.

The waveform model includes examples of narrowband interference generated by users of the HF band as well as unintentionally radiated noise generated by electrical machinery, automobile ignitions, etc. The modeling of these man-made forms of noise and interference are the subject of the present paper. The development of a model of wideband HF atmospheric noise will be discussed elsewhere.

Past developments of noise and interference models have often been directed toward statistical descriptions of the noise and interference processes, such as amplitude probability distributions. Statistical models are useful for theoretical predictions of system performance. For example, if one wishes to derive an expression of the probability of a bit error as a function of signal-to-noise ratio, one needs an expression for the probability distribution of the instantaneous value of the received noise envelope. The models developed by Middleton [1972, 1977] are well-known examples of this approach.

The present model development has been motivated by the need for a model that can be implemented in a wideband HF channel simulator to be used for laboratory measurements of radio performance. The model is therefore a description of the noise and interference waveform itself, since it is the waveform that must be added to the desired signal in a channel simulator. However, comparisons of the statistical characteristics of measured and simulated waveforms are useful for the development and validation of a waveform model.

This paper is not subject to U.S. copyright. Published in 1997 by the American Geophysical Union.

Paper number 96RS03204.

2. Data Analysis

As part of its experimental wideband HF communications program, the Mitre Corporation has obtained recordings of wideband HF noise and interference at a variety of times of day and frequencies in the HF band. The equipment used in these experiments is described by *Perry and Rifkin* [1989]. A horizontally polarized log periodic antenna (H/LPA) was used at the receive terminal when the data discussed in this paper were obtained. The H/LPA has a directivity of about 10 dBi.

The wideband receiver converts the signal from RF to baseband where the complex (inphase and quadrature) components are low-pass filtered with a cutoff frequency of 400 kHz, resulting in an equivalent RF bandwidth of 800 kHz, and digitized at a sampling rate of 1.024 MHz. Eight-bit analog-to-digital (A/D) converters were used.

The data that were analyzed in this work consist of 42 1-s records of the digitized, baseband inphase (I) and quadrature (Q) components of the received noise and interference. The data were collected during March 1989 in Bedford, Massachusetts.

To analyze these data, software was developed to compute first- and higher-order statistics of the measured waveforms. The computed first-order statistics, which characterize the time-averaged behavior of the noise and interference processes, include probability distributions of the raw data (I and Q) and of the amplitude and phase of the recorded waveforms, as well as amplitude and phase distributions of the spectra (Fourier transforms) of the waveforms. In addition, distributions of the average level crossing rate of the noise and interference envelope were computed.

Higher-order statistics of the waveforms are necessary to characterize the relationships between the noise and interference processes at different instants in time. The higher-order statistics that were analyzed include power spectra, autocorrelation functions, and pulse width and pulse spacing distributions. These quantities are precisely defined in the examples discussed below.

3. Noise and Interference Model

On the basis of computed first- and higher-order statistics of the measured waveforms, it was concluded that man-made processes generate a noise and interference waveform that can be represented as a sum of three components [*Lemmon and Behm*, 1991,

1993]: white Gaussian noise, narrowband interferers (sine waves) and impulsive man-made noise (filtered impulses).

A noise and interference waveform that comprises these three components is to be expected on heuristic grounds. Within a bandwidth of the order of 1 MHz many independent processes contribute to the noise and interference. Therefore one expects a Gaussian component as a consequence of the central limit theorem. However, interference in the HF band is generated by other users of the spectrum in the form of intentionally radiated narrowband signals, and if one or a few of these signals are dominant, as is often the case, the central limit theorem no longer holds and these interferers must be added to the model as a separate component. Finally, broadband, man-made noise is generated in the form of incidental radiation from electrical devices, automobile ignitions, electric power lines, etc. These forms of noise tend to be impulsive in nature and are therefore neither Gaussian nor narrowband and must be included as an additional component of the model.

If the noise and interference waveform at RF is denoted by $x(t)$, and the inphase and quadrature baseband components are denoted by $I(t)$ and $Q(t)$, respectively, then $x(t)$ can be written as

$$x(t) = I(t) \cos \omega_0 t + Q(t) \sin \omega_0 t, \quad (1)$$

where ω_0 is the RF center frequency. Use of the representation in (1) implies that the noise and interference is a narrowband process (bandwidth less than the center frequency) with a well-defined amplitude and phase. It may therefore seem inappropriate to refer to the noise and interference as "wideband." However, the term wideband is used in the sense that one is dealing with bandwidths of the order of 1 MHz as opposed to bandwidths of the order of several kilohertz.

The complex, equivalent low-pass waveform,

$$z(t) = I(t) + iQ(t), \quad (2)$$

can be written as

$$z(t) = g(t) + \sum_{i=1}^{N_i} A_i e^{-i(\Delta\omega_i t + \phi_i)} + \sum_{j=1}^{N_j} B_j \frac{\sin 2\pi B(t - t_j)}{t - t_j} e^{i\omega_0 t_j}. \quad (3)$$

In (3), $g(t)$ is a complex, zero-mean, white Gaussian process, $\Delta\omega_i$ are the baseband frequencies of the narrowband interferers ($\Delta\omega_i = \omega_i - \omega_0$), A_i are the amplitudes of the interferers, ϕ_i are random phases, N_i is the number of interferers in the frequency band of interest, t_j are the arrival times of the filtered impulses, B_j are the amplitudes of the impulses, B is the bandpass (in hertz) of the (square) low-pass filter in the HF receiver, and N_j is the number of impulses in the time interval during which the noise and interference are being modeled.

Still to be specified are the fractions of the total noise and interference power that are associated with each of the three components of the model, the numbers of narrowband interferers and filtered impulses, the distributions of the narrowband interferers in amplitude, frequency, and phase, and the distributions of the filtered impulses in amplitude, time, and phase. To specify these quantities, the statistics of measured waveforms were examined and compared with the statistics of waveforms simulated with the model.

It was concluded that the frequency and phase distributions of the narrowband interferers are uniform and that the amplitude distribution of the narrowband interferers can be described by a model developed by *Hall* [1966] for impulsive noise. Although it may seem inappropriate to use a model of impulsive phenomena to characterize narrowband interferers, these interferers are impulsive in the frequency domain, and it is the amplitude distribution of these frequency domain impulses that must be described.

The probability density function $p_A(A)$ for the amplitudes A_i is

$$p_A(A) = (\theta_A - 1)\gamma_A^{(\theta_A - 1)} A / (A^2 + \gamma_A^2)^{(\theta_A + 1)/2}, \quad (4)$$

where θ_A and γ_A are free parameters (with the constraint that $\theta_A > 1$, so that $p_A(A)$ is normalizable). The Hall distribution in (4) was chosen because, as shown in the examples below, it leads to a noise and interference waveform whose spectral properties closely resemble those of the measured data. A set of amplitudes distributed according to (4) can be generated by integrating (4) to obtain the cumulative probability $P(A)$,

$$P(A) = 1 - \gamma^{(\theta_A - 1)} / (A^2 + \gamma_A^2)^{(\theta_A - 1)/2}, \quad (5)$$

inverting the result to obtain $A(P)$,

$$A(P) = \gamma[(1 - P)^{1/(1 - \theta_A)}], \quad (6)$$

and treating the cumulative probability P as a random variable uniformly distributed between 0 and 1.

Analyses of the first-order statistics of the man-made noise observed in the data indicated that the distribution of the amplitudes B_j of the filtered impulses can also be described by the Hall model for amplitudes that are less than some maximum value B_{\max} , and that the distribution be cut off for amplitudes greater than B_{\max} :

$$p_B(B) = \begin{cases} \frac{1 - \theta_B}{(B_{\max}^2 + \gamma_B^2)^{(1 - \theta_B)/2} - \gamma_B^{2(1 - \theta_B)/2}} \cdot \frac{B}{(B^2 + \gamma_B^2)^{(\theta_B + 1)/2}}, \\ 0 \leq B \leq B_{\max} \\ B > B_{\max} \end{cases}, \quad (7)$$

where θ_B and γ_B are free parameters (with $\theta_B > 1$). The expression in the first line of (7) differs from that in (4) because cutting off the distribution results in a different normalization constant. The amplitudes B_j can be generated by a technique analogous to that used to generate the A_i , that is, by integrating (7) to obtain the cumulative distribution $P(B)$,

$$P(B) = \frac{(B^2 + \gamma_B^2)^{(1 - \theta_B)/2} - \gamma_B^{2(1 - \theta_B)/2}}{(B_{\max}^2 + \gamma_B^2)^{(1 - \theta_B)/2} - \gamma_B^{2(1 - \theta_B)/2}}, \quad (8)$$

inverting (8) to obtain $B(P)$,

$$B(P) = \gamma_B \left(\left\{ P \left[\left(\frac{B_{\max}^2}{\gamma_B^2} + 1 \right)^{(1 - \theta_B)/2} - 1 \right] + 1 \right\}^{2/(1 - \theta_B)} - 1 \right)^{1/2}, \quad (9)$$

and treating P as a random variable uniformly distributed between 0 and 1.

Analyses of the pulse width and pulse spacing distributions of the man-made noise that was observed indicated that the noise pulses are not distributed uniformly in time, but that they are clustered in bursts and that the bursts are correlated in time. These features can be simulated by treating the arrival times t_j of the filtered impulses as a uniformly distributed random variable within windows of 4 μ s duration and the time interval between windows as a random variable uniformly distributed between 450 and 550 μ s.

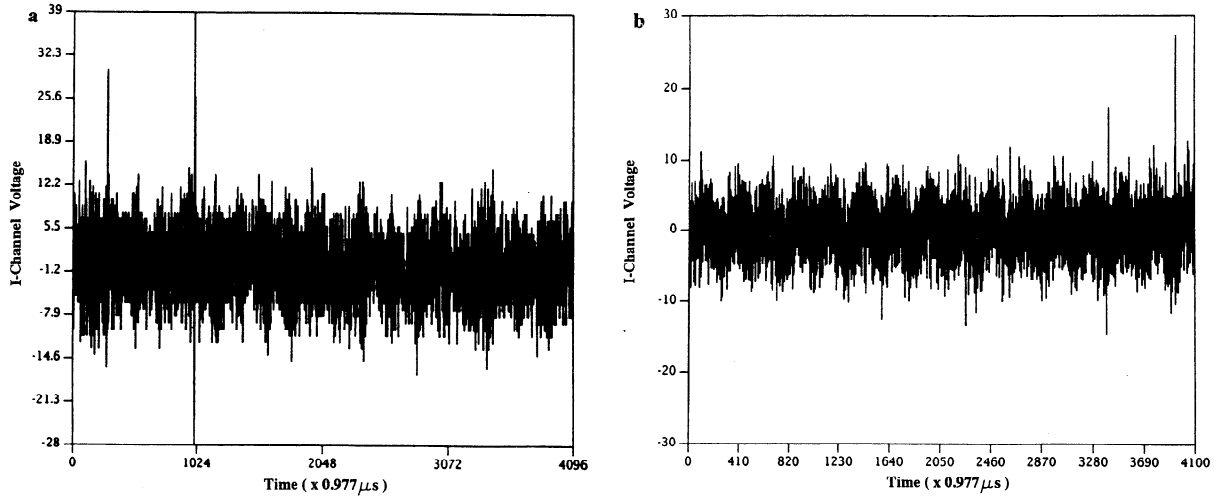


Figure 1. Comparison of (a) measured and (b) simulated I channel data.

4. Comparisons of the Model With Measurements

The model development discussed above has been based on numerous analyses and detailed case studies too lengthy for a complete presentation herein. The comparisons of the model with measurements will therefore be restricted to a variety of first- and higher-order statistics of one particular case study. This particular case has been chosen because, of the 42 noise and interference records examined, only this case clearly exhibits man-made impulsive noise in the raw data, and it is therefore of greatest generality. The data were obtained at 1922:31 UT on March 15, 1989, at a center frequency of 23.862 MHz.

A plot of the first 4 ms of the I channel data is shown in Figure 1a. The origin of the noise pulses is unknown but is almost certainly not atmospheric noise because the noise pulses tend to occur in a quasi-periodic fashion, as revealed by the pulse spacing distributions discussed below. Thus the (unknown) source of the noise has been assumed to be of man-made origin.

In this particular noise record the quantization of the noise samples is apparent. This is presumably because the gain of the HF receiver was decreased to prevent the noise pulses from saturating the system, so that the voltage level of the noise floor was comparable to the resolution of the A/D converters.

Figure 1b shows a plot of the first 4 ms of the I channel voltage of a noise and interference waveform that was simulated using the model. The waveform is

a combination of complex, zero-mean, white Gaussian noise, 40 sine waves, and 50 filtered impulses in each 4-ms block, resulting in a total of 12,500 impulses in the entire 1-s simulation. The real and imaginary parts of the complex Gaussian noise both have a variance $\sigma^2 = 0.0144$. The parameters in the amplitude distributions of the sine waves and the filtered impulses are $\theta_A = 2.0$, $\gamma_A = 0.2$, $\theta_B = 1.2$, $\gamma_B = 1.0 \times 10^{-8}$, and $B_{\max} = 2.0 \times 10^{-5}$. The parameter B in (3) is equal to 400 kHz, corresponding to an equivalent RF bandwidth of 800 kHz. These values of the model parameters were obtained by comparing the statistics of the measured and simulated waveforms.

4.1. First-Order Statistics

The cumulative distribution functions of the power envelope ($I^2 + Q^2$) of the first 4 ms of the measured and simulated waveforms are shown in Figure 2. Plotted is the (common) logarithm of the probability that the power exceeds some threshold as a function of that threshold in decibels.

The distributions exhibit two distinct regimes, separated by a transition region where the logarithm of the exceedence probability is approximately -2.5 . The regime at the lower power levels comprises the Gaussian noise, the narrowband interferers, and the impulsive noise, whereas the regime at the higher power levels corresponds only to the impulsive noise.

The power in the Gaussian, narrowband, and impulsive components can be computed by evaluating

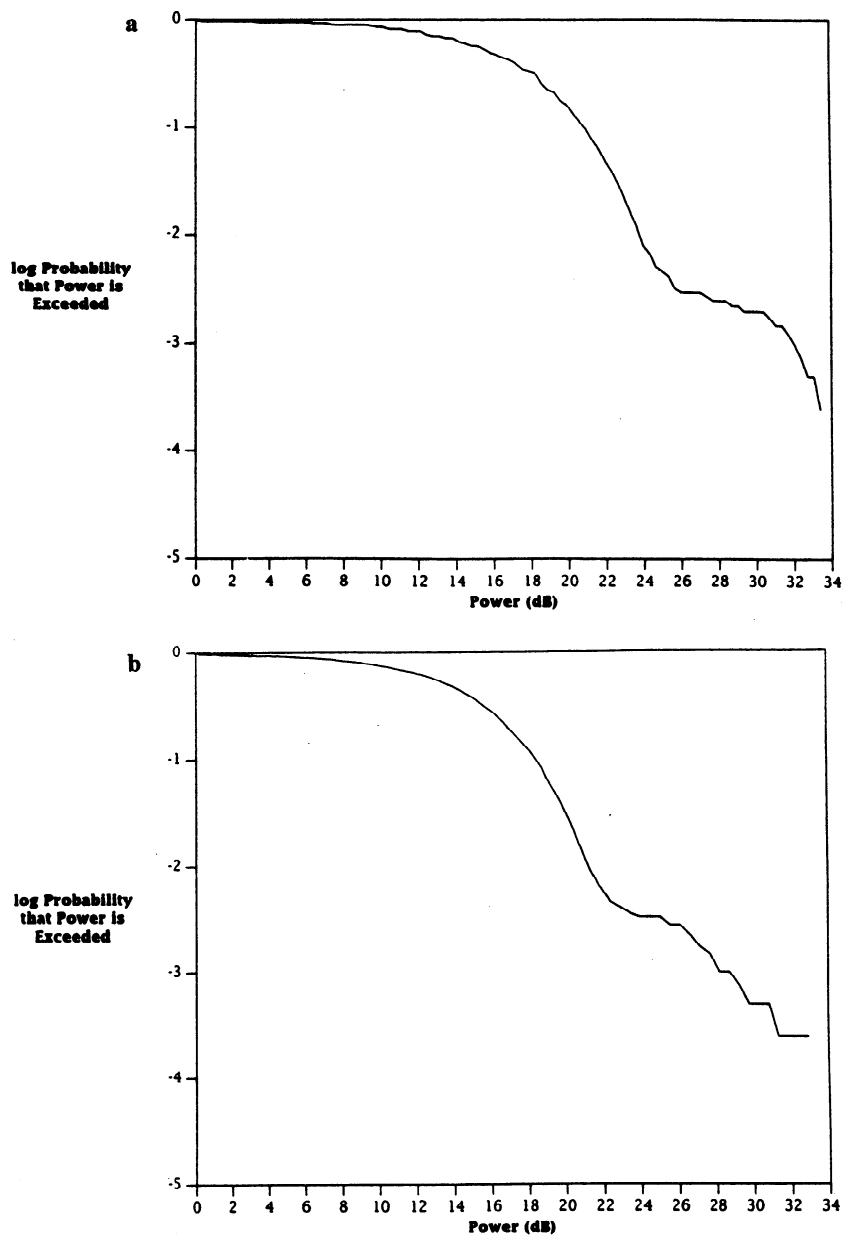


Figure 2. Comparison of (a) measured and (b) simulated cumulative distribution functions of the power envelope in the time domain.

the time average of $I^2 + Q^2$ and ignoring the cross terms between different components, since the three components are independent processes and the Gaussian and narrowband components are zero-mean processes. The average power in the Gaussian component is

$$P_G = \frac{1}{T} \int_0^T |g(t)|^2 dt = 2\sigma^2, \quad (10)$$

where T is the record length, σ^2 is the variance of the real and imaginary components of $g(t)$, and the cross term between the real and imaginary components of

$g(t)$ has been ignored since these components are independent, zero-mean processes. The power in the narrowband component is

$$P_{NB} = \frac{1}{T} \int_0^T \left| \sum_{i=1}^{N_i} A_i e^{-i(\Delta\omega_i t + \phi_i)} \right|^2 dt \quad (11)$$

$$= \sum_{i=1}^{N_i} A_i^2,$$

where the integral over the cross terms in (11) vanishes because of the orthogonality of sines and cosines of different frequencies. The power in the impulsive component is

$$P_{IMP} = \frac{1}{T} \int_0^T \left| \sum_{j=1}^{N_j} B_j \frac{\sin 2\pi B(t - t_j)}{t - t_j} e^{i\omega_0 t_j} \right|^2 dt$$

$$\approx \frac{2\pi^2 B}{T} \sum_{j=1}^{N_j} B_j^2 \int_{-\infty}^{\infty} \frac{\sin^2 \pi x}{\pi^2 x^2} dx = \frac{2\pi^2 B}{T} \sum_{j=1}^{N_j} B_j^2, \quad (12)$$

where the cross terms in (12) that arise from the products of two distinct impulses are assumed to approximately vanish, and where the integral from 0 to T has been approximated by the integral from $-\infty$ to $+\infty$.

In the simulated waveform, $\sigma^2 = 0.0144$, $\sum A_i^2 = 28.13$, $\sum B_j^2 = 1.26 \times 10^{-9}$, $B = 400$ kHz, and $T = 4$ ms. Substituting these values into (10) through (12), one finds that $P_G = 0.0288$, $P_{NB} = 28.13$, and $P_{IMP} = 2.52$. Thus, relative to the Gaussian noise power, the narrowband power is approximately 30 dB and the impulsive power is approximately 19 dB.

Probability density functions of the phase ($\tan^{-1}(Q/I)$) of the first 4 ms of the measured and simulated waveforms are shown in Figure 3 in the form of histograms. The spikes in the phase distribution of the measured data are an artifact that arises because of the aforementioned quantization of the data. Because the I and Q channel voltages are integral multiples of a fundamental voltage (the resolution of the A/D converters), the phase is discretized at values equal to the arctangent of the ratio of two integers. Thus one expects peaks in the phase distribution at $\tan^{-1}(0/1) = 0$, $\tan^{-1}(1/0) = \pi/2$, $\tan^{-1}(1/1) = \pi/4$, $\tan^{-1}(1/2) = 0.46$, etc. These peaks are intentionally not being simulated; in fact, the simulated phase distribution closely resembles the

phase distributions of recorded waveforms that do not exhibit quantization noise.

4.2. Spectral Properties

Figure 4 shows the power spectra of the first 4 ms of the measured and simulated waveforms, computed as the absolute square of the (discrete) complex Fourier transform of the baseband data. Because the transforms are discrete transforms of 4-ms records sampled at 1.024 MHz, the power spectra span a bandwidth of 1.024 MHz with a spectral resolution of 250 Hz. The spectra have been folded so that the zero frequency at baseband (center frequency at RF) appears at the far left and right ends of the frequency scale.

The power spectra clearly reveal the presence of many narrowband interferers. The absence of these interferers from the center of the plot in Figure 4a is due to the fact that this part of the spectrum is outside the bandpass of the low-pass filter in the HF receiver. Accordingly, the baseband frequencies $\Delta\omega_i$ of the narrowband interferers in the simulated waveform are treated as a random variable uniformly distributed between -400 and $+400$ kHz. The finite spectral width of some of the sine waves in the simulated power spectrum is spectral splatter that arises when the frequency of a sine wave does not coincide with one of the frequencies in the discrete Fourier transform.

In the measured spectrum, the fact that the noise floor within the 400-kHz bandpass of the low-pass filters in the HF receiver is greater (by approximately 20 dB) than the noise floor outside the bandpass of the filters indicates that a broadband process (impulsive noise) is contributing to the inband power spectral density. This difference between the inband and out-of-band noise floors corresponds to the 19-dB difference between the Gaussian and impulsive noise powers that was computed above and can be seen in the simulated spectrum in Figure 4b.

The amplitude distribution of the narrowband interferers can be characterized by the cumulative distribution of the power spectral density, shown in Figure 5 for both the simulated and measured power spectra of Figure 4. In analogy to the cumulative distributions of power in the time domain (Figure 2), Figure 5 shows the logarithm of the probability that the power in a spectral bin exceeds some threshold plotted versus that threshold in decibels. Like the distributions in Figure 2, the distributions in Figure 5 reveal two different regimes. Here, however, the

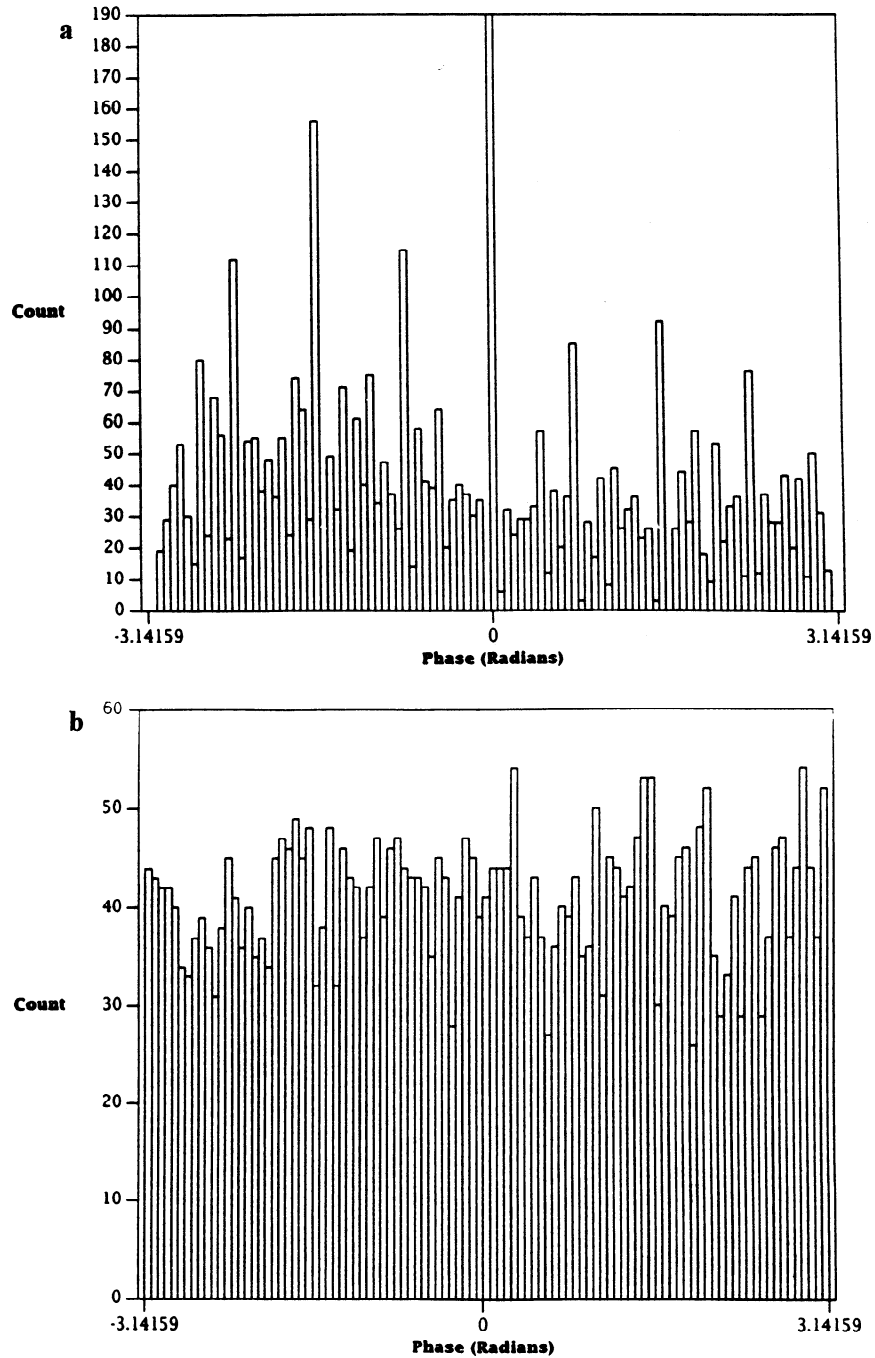


Figure 3. Comparison of (a) measured and (b) simulated probability density functions of the phase in the time domain.

regime at the higher power levels (greater than approximately 55 dB) comprises only the narrowband interferers. The approximately linear character of the distribution in this regime was observed in the other

noise and interference records that were analyzed and has also been reported by *Perry and Abraham* [1988] and *Mousley* [1985].

Probability density functions of the phase of the

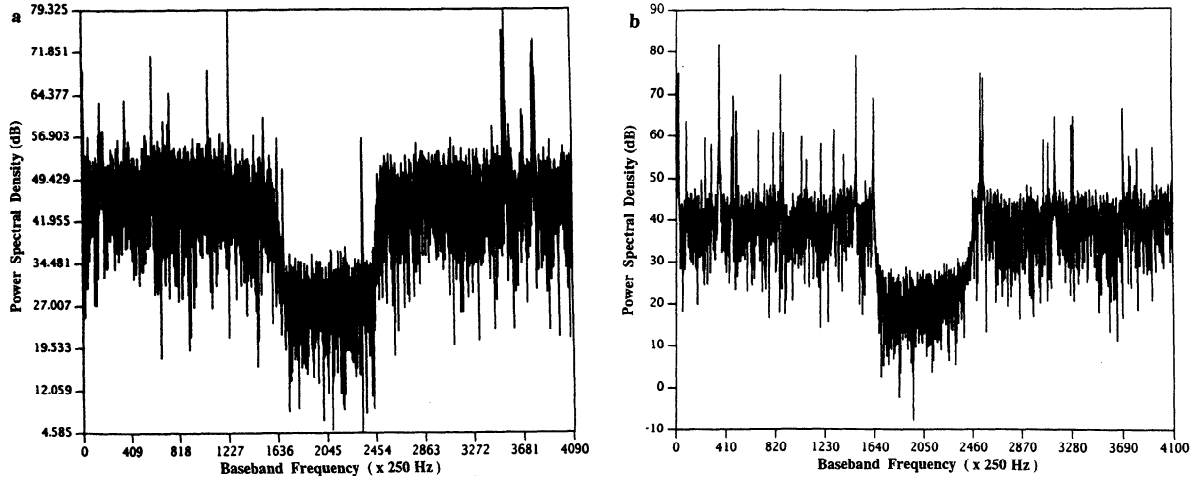


Figure 4. Comparison of (a) measured and (b) simulated power spectra.

measured and simulated spectra are shown in the form of histograms in Figure 6. Unlike the time domain phase distributions, which are approximately uniform for all the noise and interference records that were analyzed, the frequency domain phase distributions are decidedly nonuniform. This nonuniformity can be understood as follows.

The Fourier transform of a complex, zero-mean, white Gaussian process is another zero-mean Gaussian process; the transform of a sum of sine waves is a sum of impulses with Hall-distributed amplitudes; the transform of a sum of impulses (with different arrival times) is a sum of sine waves (with different frequencies). A combination of sine waves and Gaussian noise results in a Ricean process, whose phase distribution is well known to be nonuniform [Papoulis, 1965]. Similarly, the phase distribution of a process that is a combination of Gaussian noise and a Hall-distributed process can be shown to be nonuniform [Lemmon and Behm, 1991], as can the phase distribution of a process comprising all three components (Gaussian noise, sine waves, and impulses). The point is that although the phase distributions of the individual components are uniform, the phase distribution of the composite process is not.

This argument is equally applicable to the time domain waveform, which also consists of Gaussian noise, sine waves, and impulses. In fact, the time domain phase distributions are approximately but not precisely uniform. No attempt has been made to quantify this difference between the phase distributions in the time and frequency domains. What is

important is that the measured and simulated distributions are qualitatively similar to one another in both domains for a variety of noise and interference environments.

Closely related to the power spectrum of a random process is its autocorrelation function, which has been computed as

$$R(\tau, t) = \frac{1}{T} \int_0^T z^*(t)z(t + \tau) dt. \quad (13)$$

An analytic expression for $R(\tau, T)$ in the noise and interference model can be obtained by substituting (3) into (13). Note that $R(0, T)$ is the average power of the noise and interference process, given by (10) through (12). For nonzero values of τ , arguments similar to those used in the derivation of (10) through (12) can be used to evaluate (13). The result is

$$R(\tau, T) = \left(2\sigma^2 + \frac{2\pi^2 B}{T} \sum_{j=1}^{N_j} B_j^2 \right) \delta_{\tau,0} + \sum_{i=1}^{N_j} A_i^2 e^{-i\Delta w_i \tau}, \quad (14)$$

where $\delta_{\tau,0}$ is an impulse function, defined as

$$\delta_{\tau,0} = \begin{cases} 1, & \tau = 0 \\ 0, & \tau \neq 0 \end{cases}. \quad (15)$$

Thus $R(\tau, T)$ is the sum of an impulse at $\tau = 0$ and a periodic function of τ .

The autocorrelation functions of the simulated and measured waveforms discussed in the previous exam-

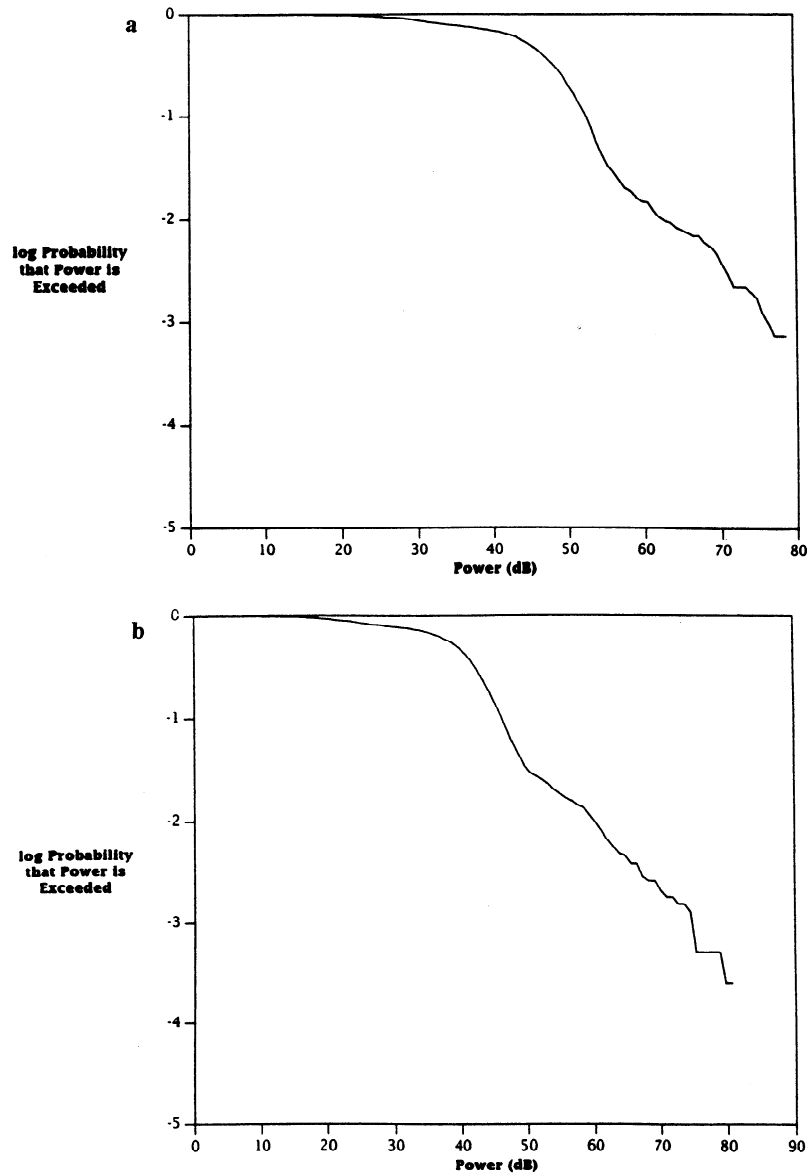


Figure 5. Comparison of (a) measured and (b) simulated cumulative distribution functions of the power envelope in the frequency domain.

ples are shown in Figure 7 for $0 \leq \tau \leq 4$ ms. The integration time T was chosen to be 4 ms (i.e., 4096 samples). Because one expects an impulse in $R(\tau, T)$ at $\tau = 0$, which is difficult to see on the plots, the autocorrelation functions were normalized so that $R(0, T) = 1$. Because $R(\tau, T)$ is complex, the absolute magnitudes of the normalized autocorrelation functions have been plotted. Thus the quantity that has been plotted in each case is $|R(\tau, T = 4 \text{ ms})/R(0, T = 4 \text{ ms})|$.

As expected, the normalized autocorrelation func-

tions consist of a unit impulse at $\tau = 0$, followed by an approximately periodic function of τ . The simulated autocorrelation function does not resemble the measured function in quantitative detail; the difficulty in achieving quantitative agreement arises from the fact that one is dealing with random processes and therefore an infinite variety of waveforms. Thus the frequencies and amplitudes of the narrowband interferers (which determine the nature of the autocorrelation function for nonzero values of τ) have been

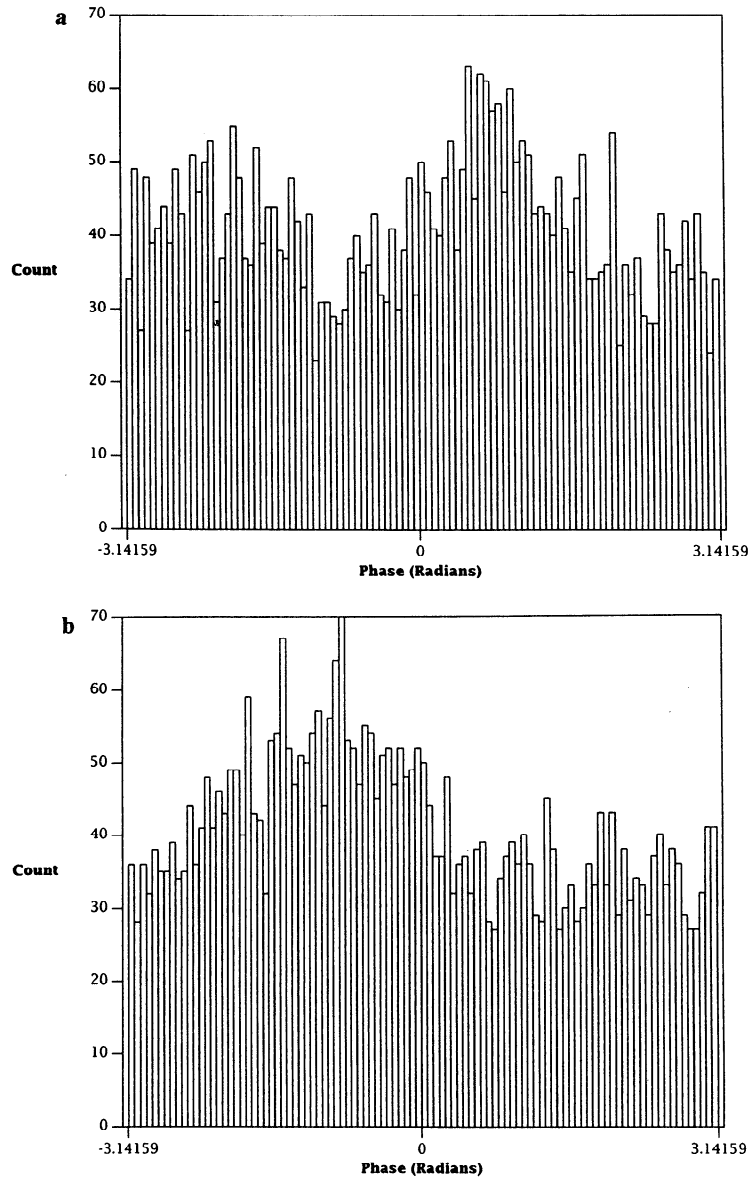


Figure 6. Comparison of (a) measured and (b) simulated probability density functions of the phase in the frequency domain.

treated as random variables in the simulated waveform and do not correspond to those of the measured waveform. However, using the expression in (14) for guidance, it has been shown that the wide variety of autocorrelation functions of the measured data can be simulated using the model with appropriate choices for the amplitudes and frequencies of the dominant interferers [Lemmon and Behm, 1993].

4.3. Level Crossing Distributions

Figure 8 shows level crossing distributions of the simulated and measured waveforms. Plotted is the number of upgoing crossings (in a time interval of 4 ms) of the voltage envelope $((I^2 + Q^2)^{1/2})$ across a given threshold as a function of that threshold. Thus the number of crossings divided by 4 ms gives the average level crossing rate in crossings per second.

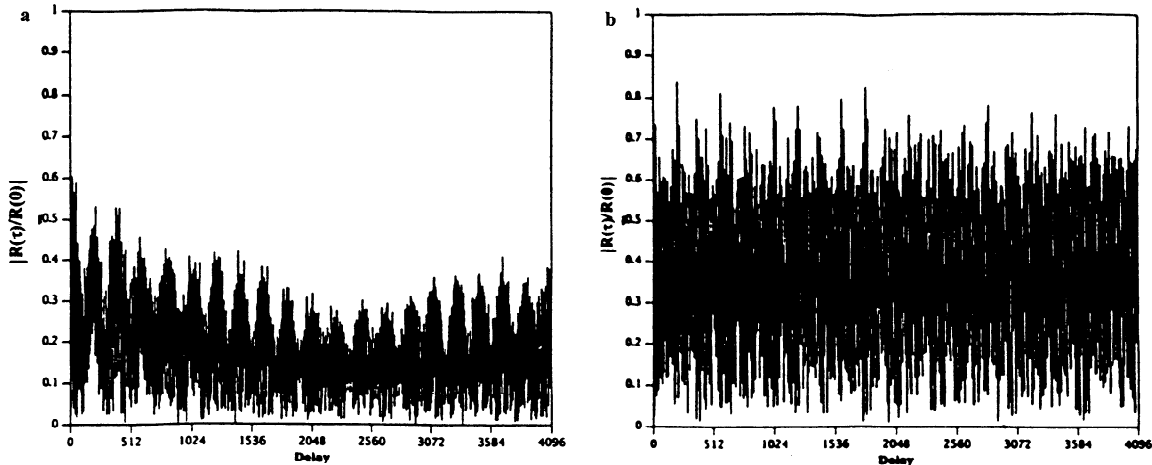


Figure 7. Comparison of (a) measured and (b) simulated normalized autocorrelation functions.

The tails in the distributions at high thresholds correspond to the impulsive noise bursts.

The similarity of the distributions in Figure 8 indicates that the envelopes of the simulated and measured waveforms fluctuate at the same average rate in time. Characterization of the precise nature of these fluctuations, that is, the relationships between the envelope at different instants in time, requires investigation of the higher-order statistics. In particular, the pulse width and pulse spacing distributions need to be examined.

Pulse width is defined as the time interval between an upgoing crossing of the voltage envelope through some threshold and the next downgoing crossing of the envelope through that same threshold. Conversely, pulse spacing is defined as the time interval between a downgoing crossing of the envelope through some threshold and the next upgoing crossing through that threshold. Thus, for a given data record, a family of distributions (corresponding to various thresholds) is required to characterize the distributions of pulse widths and pulse spacings.

Figures 9 and 10 show pulse width distributions of the measured and simulated waveforms, respectively, for thresholds of 5 and 30. Pulse spacing distributions of the waveforms for these same thresholds are shown in Figures 11 and 12. Each point in Figures 9–12 corresponds to the number of occurrences of a pulse width (spacing) of a given time duration. To obtain a sufficient number of occurrences to clearly reveal the trends in the distributions, it was necessary to analyze the entire 1-s records. The scales are logarithmic

because of the large ranges of values that were encountered.

The pulse width and spacing distributions are especially helpful for modeling the impulsive noise bursts. For example, the measured pulse width distribution at a threshold of 30 reveals numerous pulse widths between 2 and 10 μs , whereas the base width of the central lobe of an impulse filtered with a 400-kHz low-pass filter is 2.5 μs . A pulse width greater than 2.5 μs at high thresholds can be achieved either by filtering an impulse with a bandpass less than 400 kHz or by superimposing two or more impulses. However, the measured pulse spacing distribution at a threshold of 30 reveals numerous pulse spacings of the order of or less than 10 μs , which is indicative of fine structure in the pulses, suggesting that the noise bursts consist of superpositions of individual impulses. This has been verified by inspection of the voltage envelope on an expanded time-scale [Lemmon and Behm, 1993].

The measured pulse spacing distribution at a threshold of 30 also exhibits a bump in the vicinity of 500 ps, indicating that the noise bursts tend to occur periodically in time. However, the bumps have finite widths, indicating that the bursts are not precisely periodic. Thus the level crossing distributions reveal both fine structure and time correlations associated with the noise bursts, which have been taken into account in modeling the impulsive noise.

The simulated distributions at thresholds of 30 in Figures 10 and 12 typically have fewer occurrences associated with these features than do the measured

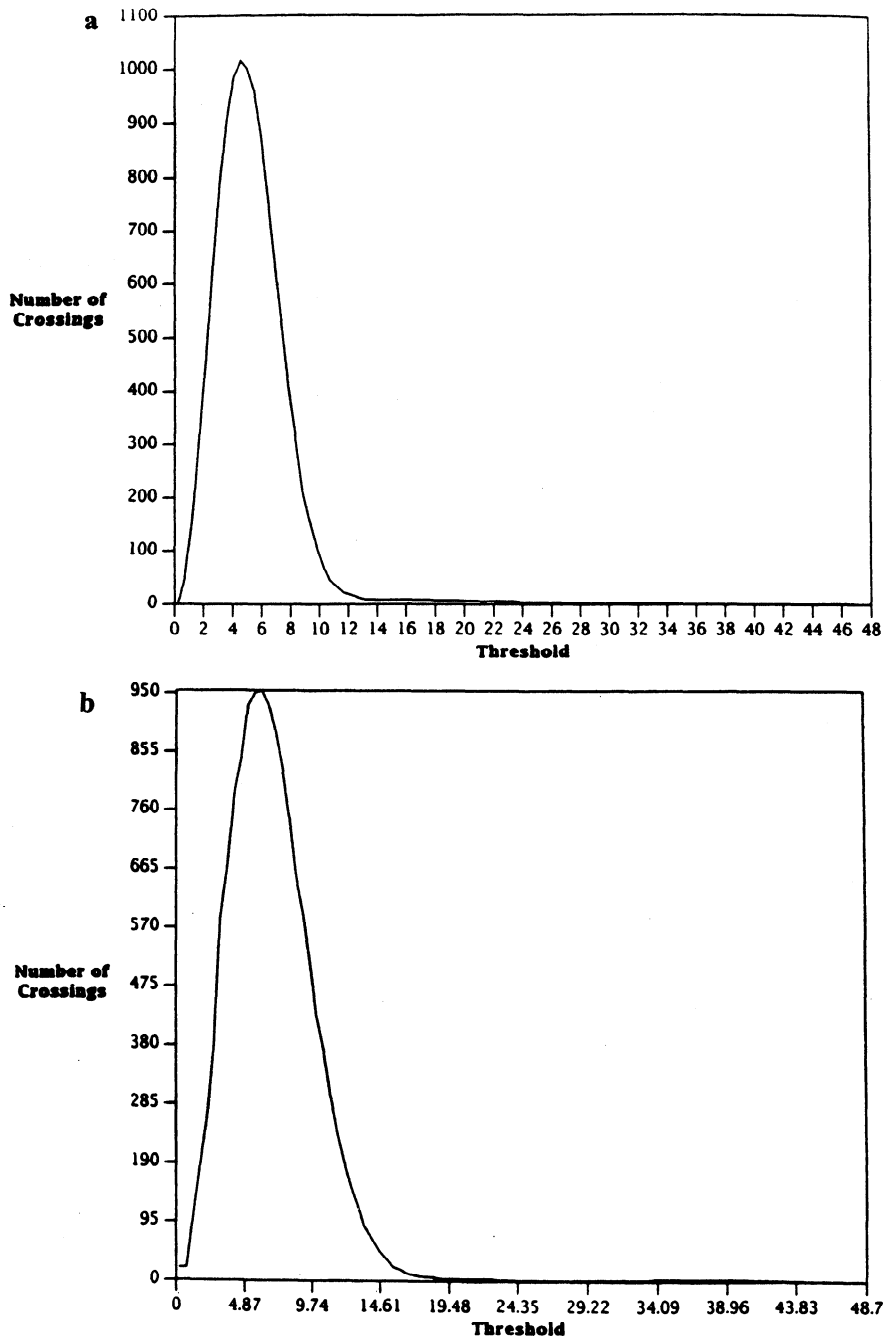


Figure 8. Comparison of (a) measured and (b) simulated level crossing distributions of the voltage envelope.

distributions. These differences in the number of occurrences could be diminished by simulating the impulsive noise with a greater number of impulses. One could also envisage a more sophisticated mod-

eling of the arrival time distribution of the impulses to more accurately reproduce the shapes of these features.

The level crossing distributions also indicate that the impulsive noise is not atmospheric noise. Light-

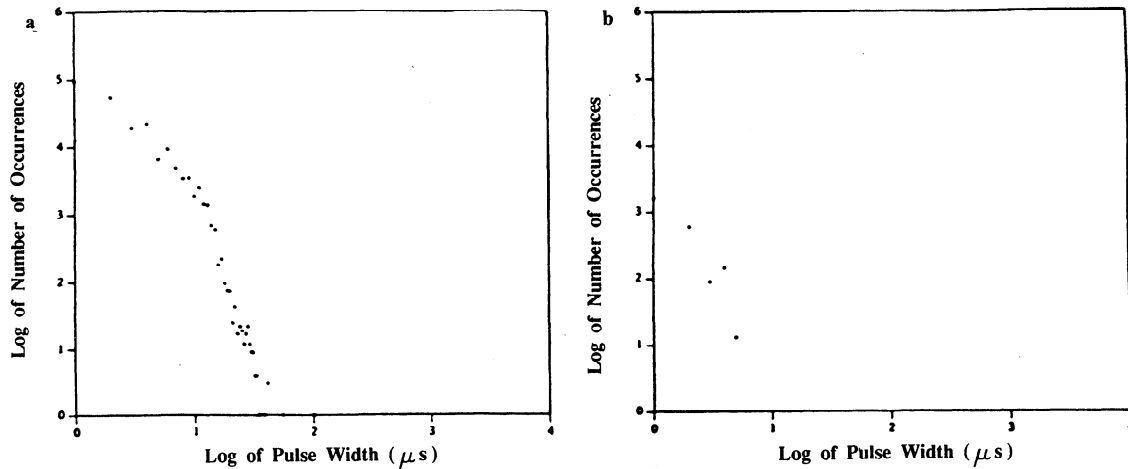


Figure 9. Measured pulse width distributions at thresholds of (a) 5 and (b) 30.

ning flashes comprise one or more strokes with pulse widths of the order of $100 \mu s$ and with spacings between strokes of the order of tens of milliseconds [Uman, 1987]. On the other hand, the level crossing distributions reveal pulse widths of the order of several microseconds and pulse spacings of the order of half a millisecond.

5. Conclusions

A simple model of the waveform of man-made HF noise and interference has been described. The model development has been based on analyses of recorded waveforms over an equivalent RF bandwidth of 800 kHz at various times of day and frequencies in the HF

band (3–30 MHz). Examples of first- and higher-order statistics of the recorded waveforms have been compared with those generated by the model. These comparisons are of a qualitative nature. Quantitative comparisons are difficult because one is dealing with an infinite variety of waveforms generated by random processes.

Ideally, a database used for model development would be obtained from many geographical locations and various seasons, whereas the data discussed in this paper were all obtained at a single site (Bedford, Massachusetts) during March 1989. Nevertheless, the general structure of the model (narrowband interferers, filtered impulses, and a Gaussian noise back-

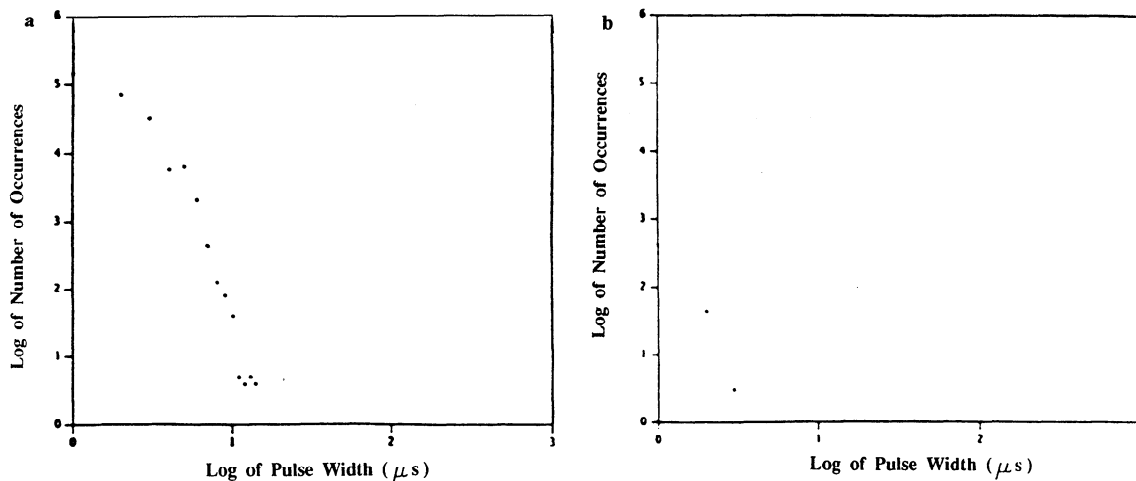


Figure 10. Simulated pulse width distributions at thresholds of (a) 5 and (b) 30.

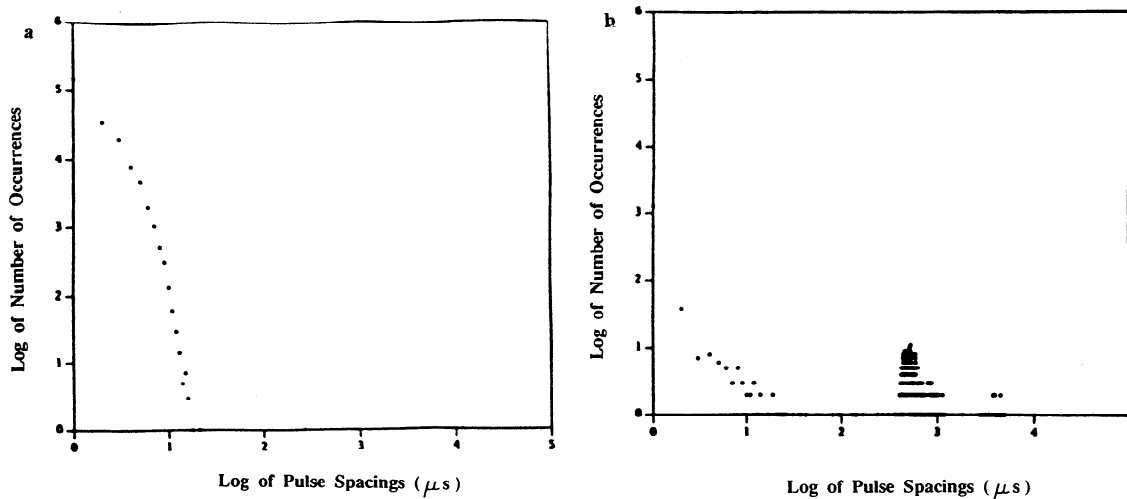


Figure 11. Measured pulse spacing distributions at thresholds of (a) 5 and (b) 30.

ground) is expected to be applicable to a wide range of environments. For example, limited analyses of data obtained by Mitre during a European measurements campaign revealed a spectrum considerably more congested with narrowband interference than the Bedford data; however, increasing the number of interferers in the model from 50 to 200 resulted in a cumulative distribution function of the power spectral density that showed good agreement with the measured data.

To mention a second example, only one case of impulsive manmade noise was analyzed in detail. Examination of the pulse width and spacing distribu-

tions revealed a "bursty" distribution for the times of arrival of the impulses that can be simulated by clustering the impulses in bursts that are correlated in time. It is expected that this general approach could be used to model other forms of impulsive man-made noise as well.

Noise and interference in the HF band can be highly nonstationary (for example, when dominant interferers drop in and out of the spectrum), and this nonstationarity has not been incorporated into the model. However, the motivation of the work reported herein has been to develop the capability to perform laboratory measurements of radio performance un-

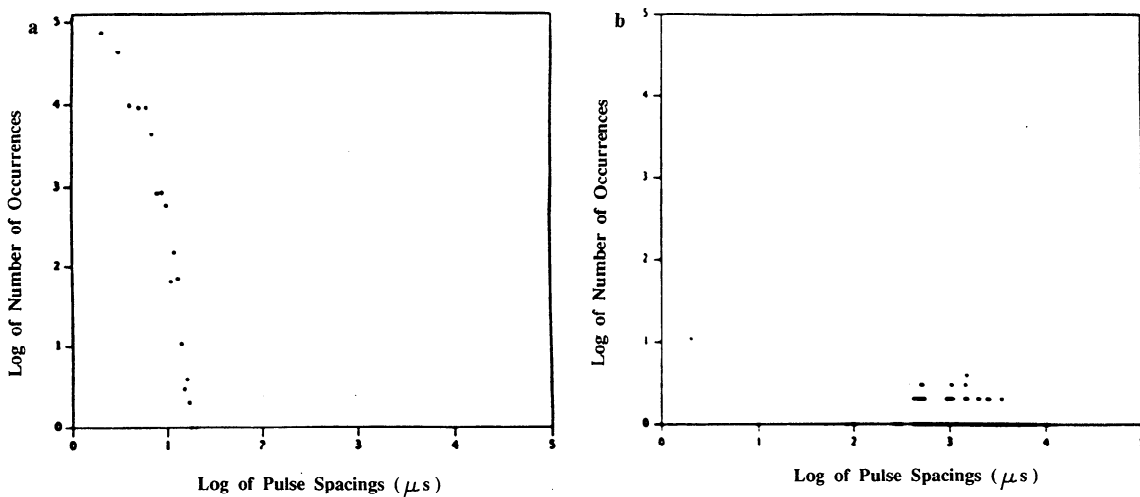


Figure 12. Simulated pulse spacing distributions at thresholds of (a) 5 and (b) 30.

der stationary channel conditions so that performance and channel conditions can be correlated. From this point of view, the lack of nonstationarity is not a serious limitation of the model.

Finally, the atmospheric noise waveform has not been discussed in this paper. However, a wideband model of HF atmospheric noise has been developed and will be reported elsewhere.

Acknowledgments. The author wishes to thank J. McEvoy and W. Bonser of the U.S. Air Force Rome Laboratory, D. Bodson and G. Rekstad of the National Communications System, and LTC Robert Oldham of the U.S. Army Communications/Electronics Command for their support of the work reported herein. The author also wishes to thank M. N. Richard of the Mitre Corporation for his generosity in sharing noise/interference data collected with the Mitre wideband HF test facility.

References

- CCIR (International Radio Consultative Committee), HF ionospheric channel simulators, *CCIR Rep. 549-2*, Int. Telecommun. Union, Geneva, Switzerland, 1986.
- Hall, H. M., A new model of "impulsive" phenomena: Applications to atmospheric noise communications channels, *Tech. Rep. 3412-8 and 7050-7, SU-SEL-66-052*, Electron. Lab., Stanford Univ., Stanford, Calif., 1966.
- Lemmon, J. J., and C. J. Behm, Wideband HF noise/interference modeling, Part I, First-order statistics, NTIA Rep. 91-277, NTIS Order PB 91-208454, Natl. Telecommun. and Inf. Admin., Springfield, Va., 1991.
- Lemmon, J. J., and C. J. Behm, Wideband HF noise/interference modeling, Part II, Higher-order statistics, NTIA Rep. 93-293, NTIS order 93-174696, Natl. Telecommun. and Inf. Admin., Springfield, Va., 1993.
- Middleton, D., Statistical-physical models of urban radio noise environments, Part I, Foundations, *IEEE Trans. Electromagn. Compat., EMC-14*, 38-56, 1972.
- Middleton, D., Statistical-physical models of electromagnetic interference, *IEEE Trans. Electromagn. Compat., EMC-19*, 106-127, 1977.
- Mousley, T. J., HF data transmission in the presence of interference, paper presented at IEE Third International Conference on HF Communication Systems and Techniques, Inst. of Electr. Eng., London, U.K., 1985.
- Papoulis, A., *Probability, Random Variables, and Stochastic Processes*, p. 501, McGraw-Hill, New York, 1965.
- Perry, B. D., and L. G. Abraham, Wideband HF interference and noise model based on measured data, paper presented at IEE Fourth International Conference on HF Radio Systems and Techniques, Inst. of Electr. Eng., London, U.K., 1988.
- Perry, B. D., and R. Rifkin, Measured wideband HF mid-latitude channel characteristics, paper presented at IEEE Military Communications Conference, Inst. of Electr. and Electron. Eng., Boston, Mass., 1989.
- Uman, M. A., *The Lightning Discharge*, Academic, San Diego, Calif., 1987.
- Vogler, L. E., and J. A. Hoffmeyer, A model for wideband HF propagation channels, *Radio Sci.*, 28, 1131-1142, 1993.

J. J. Lemmon, U.S. Department of Commerce/NTIA/ITS.S3, 325 Broadway, Boulder, CO 80303-3328. (e-mail: jlemmon@its.bldrdoc.gov)

(Received February 23, 1996; revised September 24, 1996; accepted October 18, 1996.)